Optimization of a Heliostat Field by Multiobjective Particle Swarm Optimization (MOPSO) Algorithm Based on Energy, Exergy, and Economic Point of Views

Huijuan Zhang
City College of Science and Technology Chongqing University
Morteza Bayati
Urmia University of Technology
M. A. Ehyaei (aliehyaei@yahoo.com)
Islamic Azad University
A. Ahmadi
Iran University of Science and Technology
V. A. F. Costa
University of Aveiro

Research Article

Keywords: Heliostat, Optimization, Energy, Exergy, Economic

Posted Date: September 28th, 2021

DOI: https://doi.org/10.21203/rs.3.rs-934134/v1

Optimization of a heliostat field by multiobjective particle swarm optimization (MOPSO) algorithm based on energy, exergy, and economic point of views

Huijuan Zhang[1*], Morteza Bayati[2], M.A. Ehyaei[3*], A. Ahmadi[4], V. A. F. Costa[5]

[1] School of Civil Engineering, City College of Science and Technology Chongqing University, Yongchuan, Chongqing, 402167, China

[2] Faculty of renewable energies, Department of aerospace engineering, Urmia University of Technology, Urmia, Iran

[3] Department of Mechanical Engineering, Pardis Branch, Islamic Azad University, Pardis New City, Iran

[4] Iran University of Science and Technology, School of New Technologies, Department of Energy Systems Engineering, Iran

[5] Center for Mechanical Technology and Automation, Department of Mechanical Engineering, University of Aveiro, 3810-193 Aveiro, Portugal

Corresponding authors: sace_zhj2006@163.com, aliehyaei@yahoo.com

Abstract: This research is devoted to the energy, exergy, and economic analyses and optimization of a heliostat field. The model of the heliostat solar receiver includes detailed geometric factors related to the optical and thermal losses and efficiencies throughout the year. The main parameters of the thermal performance of this system consist of energy and exergy efficiencies, and economic parameters are investigated. By computing the energy, exergy, and economic analysis tools, they are applied for the analysis of performance, and viability of the system's operating in Tehran City, including the detailed information of the environmental conditions of that location. For optimization purposes, 7 design variables related to geometric specification of the heliostat field are selected and the related lower and upper bonds are selected. Two target functions considered for the optimization are heliostat field exergy efficiency and payback period. The economic feasibility results of this study reveal that the net present value is 58.84 million US$, the payback period is 6.76 years, and the internal rate of return is 0.16. By considering the MOPSO algorithml, the annual mean exergy efficiency is increased from the 30.9% to 34.3% while the heliostat field payback period in reduced from the 6.76 to 4.3 years.

Keywords: Heliostat; Optimization; Energy; Exergy; Economic

1. Introduction

The concentrated solar power (CSP) called the solar tower, is one promising technology to utilize solar energy. The CSP solar system is a set of mirrors with the tracking system in different lines; sometimes it is called a heliostat field [1]. This device is the core element in solar technology. The system is based on a set of mirrors rotating on two axes, reflecting and concentrating the sunlight at the top of a spot or tower. There, the sunlight turns into heat with high-temperature, which can be used to produce steam or a hot working fluid for electrical power generation[2, 3]. The thermodynamic and optical assessment of heliostat fields has been extensively reported in the literature[4-6]. The solar collector performance is affected by different types of the reflector and receiver and working fluid. In the application of this device, selecting the proper types of the working fluid, storage systems, and thermal and optical performance of the solar

receiver are very important parameters [7]. In an experimental study done by Said et al.[5], the effect of the number of mirrors on the optical performance of Fresnel heliostat was investigated. Results of this research showed that by increasing the number of mirrors, the optical efficiency of this type of heliostat was increased too. Since by variation of the number of mirrors from 7 to 9 and 11, the optical performance of this system varied to 20.65%, 27.13%, and 29.13%, respectively. Moreover, the concentration ratio of this device varied from 6.74 to 9.77 due to changing the number of mirrors from 7 to 11.

Eddhibi et al. [8] studied a heliostat field, including different losses like shadowing losses, blocking and atmospheric attenuation, and cosine loss in modeling and simulation. This study's results revealed efficiencies associated with the cosine loss, atmospheric attenuation, and shadowing and blocking losses of 82.41%, 95%, and 92%, respectively. The same investigation was conducted by other research groups, with good results' agreement [9, 10]. The optimization of a heliostat field with specified geometry was done by Talebizadeh et al. [11] to find the best achievement of the heliostat field for the maximum heat absorption of the solar receiver. Results revealed that increasing the height of the tower by 7.7% and reducing the heliostat field by 19.5% lead to about a 4% increase and a 17% decrease of the heliostat field's total efficiency and total area, respectively. The economic optimization of a heliostat field was conducted by Li et al. [12] to obtain the maximum absorbed solar energy per unit cost of the specific heliostat field (Lhasa). In this study, the unit cost of collected energy was evaluated for different parameters including radius of the field, optical parameters of the mirrors, the height of the tower, and the heliostat mirror cost. Results of this optimization showed that increasing the radial distance by 6% leads to an increase of the unit cost of collected energy from 12.49 to 12.98 $^{\mathrm{MJ}}/_{\$}$. In the optimization of a hybrid combined power cycle and the solar dish made by Saghafifar [13], the layout configuration of the heliostat was analyzed for two arrangements. Also, different economic parameters such as net present value (NPV), payback period (PP), levelised cost of electricity (LCoE), and life cycle saving, Knopf objective function were investigated for these two configurations. Results of heliostat field optimization showed that the weighted efficiency was 58.6% for the radial –staggered layout and 58.4% for the spiral layout. This study showed that the LCoE for both layouts is close to $34\ ^{\$}/_{\mathrm{MW_h}}$.

A new method was applied by Zi and Zhifeng [14] for the PS 10 location in China. In this research, the optical effects of the heliostat were investigated considering a solar tracking system in the field layout. Heliostat field different parameters including mean optical efficiency, cosine efficiency, blocking and shadowing effects, and atmospheric transmission were evaluated annually. A good agreement was obtained when comparing the results of this study with those of the existing heliostat layout. The exergy and thermo-economic study of a solar power plant with a central receiver were conducted by Toro et al. [15]. A thermodynamic and economic evaluation and optimization of this solar power plant were conducted to obtain the best exergy and economic efficiencies of the systems, reducing the exergy destruction and the exergoeconomic cost of the produced power. In other studies [16, 17], different layouts heliostat fields

including the staggered, spiral, and combinations of these two arrangements were investigated and compared. The obtained results from this research showed that the optical efficiency of the spiral layout was better than that of the staggered layout and that even the combined layout has better performance than the staggered arrangement. The energy and exergy evaluation of a system composed of a solar tower for power generation with molten salt as the working fluid was carried out for different operating and design parameters such as the type of power cycle , the direct normal irradiation (DNI), and the concentration ratio [18]. The conclusion of this research revealed that the major exergy destruction happens in the receiver system. Moreover, the results showed thermodynamics efficiency of the receiver and the whole system increased by increasing the concentration ratio and the DNI. It was also concluded that the system thermal efficiency increased if advanced power cycles were used such as reheat and supercritical Rankine cycles [18, 19]. The combination of a solar tower with an energy storage system using molten salt as the operating fluid in Chile was studied by Gallardo et al. [20]. The conclusion of this research revealed the optimal solar power plant in terms of size and configuration operating in Chile. The result was the suggestion of CSP and TES configuration. Results of this combination showed that the specific exergy cost for this system was 65.6 US$/MWh in 2018 and that this cost was estimated as 48.1 US$/MWh in 2030 [20]. The hybrid combination of CSP and TES systems was studied in several similar types of research [21]. Different parameters such as energy efficiency (ENE), exergy efficiency (EXE), and some important economic parameters such as the LCoE for different solar systems and storage units were investigated [22, 23]. Other similar researches have been carried out for the application of different operating fluids such as molten salt, thermal oil, and supercritical carbon dioxide, and inclusion of phase change materials (PCM) to increase the energy storage of the system [23, 24].

2.1. Research gap and innovation

From the previous researches, it can be concluded that although several types of research have been done about the heliostat solar receiver and integration with other systems to produce electricity, heating, and cooling,

No research in literature includes three 3E including energy, exergy, and economic analyzes in the field of solar heliostat alone and optimization with multi-objective particle swarm optimization MOPSO algorithm that considered exergy and economic aspects of this field.

Because the only energy and exergy analyses are not enough to evaluate a system and a comprehensive economic study gives a better view of choosing a system. Also, by configuration optimization of the heliostat field with the MOPSO algorithm, the system can operate with better performance with low expenses. Since no additional sub-systems are added to the heliostat field and only the geometry is changed. For this target, the heliostat solar receiver is modeled considering all the factors related to the optic and thermal losses and efficiencies during 8760 hours a year. In this work, the energy, exergy, and economic analyses of a typical heliostat solar receiver system are conducted. The model is

validated by comparing it with results obtained from the literature. Various key performance parameters such as ENE and EXE, and economic parameters such as PP, NPV, and IRR are evaluated for the system operating in Tehran City. Furthermore, by choosing two target functions (EXE and payback period), the configuration of the heliostat field is optimized.

The main innovative aspects of this study can be summarized as:

- Thermodynamic and economic analyses of a heliostat solar receiver.
- Evaluation of the exergy lost rate for each component of this typical solar receiver.
- Optimization of heliostat field by MOPSO algorithm
- Evaluation and investigation of the key parameters related to the energy and exergy performance, and economic feasibility of this system in Tehran City.

2. Methodology and model

2.1. System and process description

The schematics of the system and process under analysis are illustrated in Figure 1. Schematics of the system and process under analysis The heliostat layout is radially staggered. The circulation pump moves the working fluid (Therminol-VP1) into the system. After absorbing heat in the receiver, the working fluid is transferred to the thermal energy storage tank, the stored thermal energy being ready to be used for any useful purpose. The operating fluid convoys the thermal energy from the solar receiver to the storage tank and the storage tank providing a heat source for useful purposes.

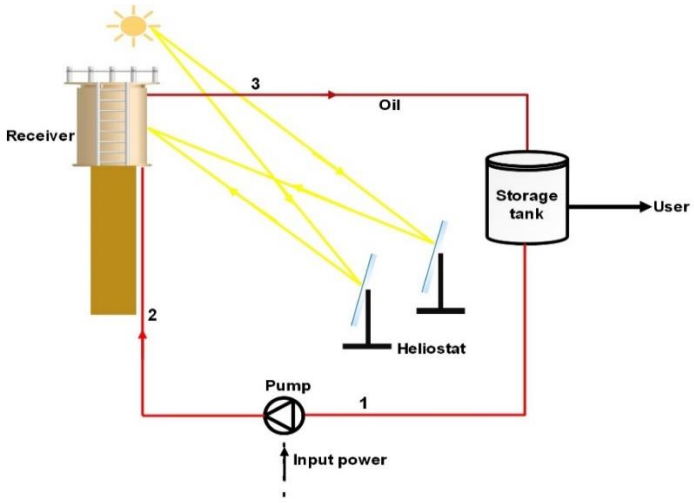

Figure 1. Schematics of the system and process under analysis

2.2. Heliostat optic modeling

The solar radiation modeling is described in Appendix A. Figure 2. The layout of heliostat field fundamentals shows the heliostat field layout's characteristics. A lot of geometrical information is required for the evaluation of how the incident solar radiation in every single heliostat reaches the receiver at the top of the tower.

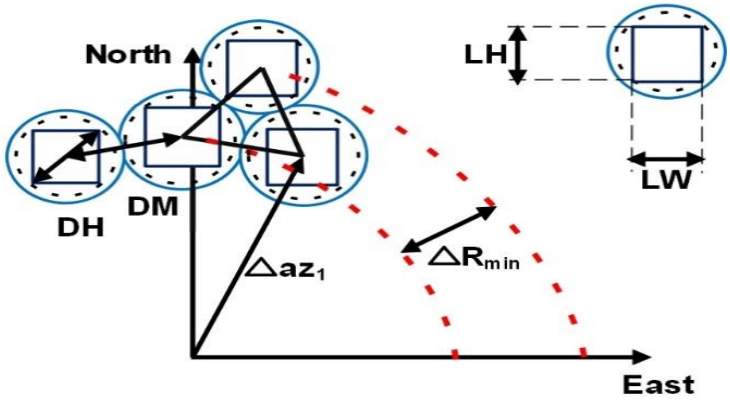

Figure 2. The layout of heliostat field fundamentals [25]

The distance between adjacent heliostats centers is the characteristic diameter that can be expressed as [26]:

$$\mathrm{DM} = \sqrt{{\mathrm{L_H}}^2 + {\mathrm{L_W}}^2} + \mathrm{desp} \tag{1}$$

where desp denotes the extra separation between adjacent heliostats, and $\mathrm{L_W}$ and $\mathrm{L_H}$ are the width and the height of the heliostat, respectively. In the first zone, the minimum radial increase of the field ($\Delta \mathrm{R_{min}}$) is obtained as [26]:

$$\Delta \mathrm{R_{min}} = \mathrm{DM}\cos(30^o) \tag{2}$$

For the heliostat field first zone, the azimuth angular spacing ($\Delta \mathrm{az_1}$) is obtained as [26]:

$$\Delta \mathrm{az_1} = 2\sin^{-1}\frac{\mathrm{DM}}{\mathrm{R_1}} \tag{3}$$

Where $\mathrm{R_1}$ is the radial distance the first row of heliostats from the tower, obtained as [26]:

$$\mathrm{R_1} = \mathrm{Nhel_1}\frac{\mathrm{DM}}{2\pi} \tag{4}$$

147 Nhel_1 is the number of heliostats *i*n the first row.

148 The distance between two adjacent mirrors is a function of the radial length from the tower as the layout
149 is radially staggered. Therefore, the farther from the tower the more space between mirrors. If this space is
150 higher than DM, installing an additional heliostat would be possible. When all these spaces have been filled
151 with additional heliostats, the field is settled. For the i^{th} field, the azimuth angular spacing is obtained as
152 [26]:

$$\Delta\mathrm{az}_\mathrm{i} = \left(\frac{\Delta\mathrm{az}_1}{2^{\mathrm{i}-1}}\right) \tag{5}$$

153 The radial distance between the first row of i^{th} field and the tower (R_i) can be obtained as [26]:

$$\mathrm{R}_\mathrm{i} = 2^{\mathrm{i}-1}\left(\frac{\mathrm{DM}}{\Delta\mathrm{az}_1}\right) \tag{6}$$

154 and for every line of i^{th} field, the number of heliostats is expressed as [26]:

$$\mathrm{Nhel}_\mathrm{i} = \left(\frac{2\pi}{\Delta\mathrm{az}_\mathrm{i}}\right) \tag{7}$$

155 For the i^{th} field, the number of heliostats rows can be obtained [26]:

$$\mathrm{Nrow}_\mathrm{i} = \left(\frac{\mathrm{R}_{\mathrm{i}+1} - \mathrm{R}_\mathrm{i}}{\Delta\mathrm{R}_{\min}}\right) \tag{8}$$

156 The heliostat optic performance is obtained as [27, 28]:

$$\eta_{\mathrm{opt}} = \rho \times \eta_{\mathrm{s\&b}} \times \eta_{\cos} \times \eta_{\mathrm{spilage}} \times \eta_{\mathrm{at}} \tag{9}$$

157 where η denotes efficiency, and subscripts s&b, cos, ref, at, and spillage are respectively shadowing and
158 blocking, cosine, $\mathrm{spilage}$, and atmospheric attenuation. ρ denotes mirror reflectivity efficiency is considered
159 to be 95% [29].

160 The cosine efficiency can be obtained by[27, 28]:

$$\eta_{\cos} = \cos[\arccos\tfrac{1}{2}(\vec{S}.\vec{R})] \tag{10}$$

161 $\vec{S}$ and $\vec{R}$ are the unit vector of incident and reflected lights.

162 The shadowing and blocking efficiency can be considered by the following relation [27, 28]:

$$\eta_{s\&b} = 1 - \frac{A_{SH}}{A_{HSR}} \tag{11}$$

163 Subscripts SH means shaded. The method of calculation of $\eta_{s\&b}$ is explained in Ref. [27].

164 The atmospheric attenuation efficiency can be expressed as [29]:

$$\eta_{at} = 0.99321 - 0.0001176\mathrm{d} + 1.97 \times 10^{-8}\mathrm{d}^2 \quad d < 1000\ m \tag{12}$$

$$\eta_{at} = \exp(-0.0001106\mathrm{d}) \qquad d > 1000\ m$$

165 Spillage efficiency can be evaluated as [30]:

$$\eta_{spillage} = \int_{-r_{ap}}^{r_{ap}} f_1 \times \mathrm{d} \tag{13}$$

166 where f_1 is obtained as [30]:

$$f_1 = \frac{1}{\sigma_1\sqrt{2\pi}} . \exp\left(-\frac{R^2}{2\sigma^2}\right) \tag{14}$$

167 where R is the space between the base of the tower and each heliostat, and σ_1 can be evaluated as [30]:

$$\sigma_1 = \frac{\mathrm{d}}{3}\sqrt{(\tan(\delta_s))^2 + (\tan(\varepsilon_{surf}))^2 + (\tan(\varepsilon_{track}))^2} \tag{15}$$

168 where ε_{track} and ε_{surf} are the errors caused by tracking and angular deviation due to surface defects, which
169 are considered to be equal to 1° and 2°, respectively [30]. δ_s denotes solar declination, evaluated in
170 Appendix A.

171 In Eq. (13) r_{ap} is the effective size of the receiver opening, which can be obtained as [30]:

$$r_{ap} = \sqrt{\frac{A_{ap}}{\pi}} \times \cos(\theta_R) \tag{16}$$

172 where θ_R denotes the angle between the vertical direction and the reflected irradiation, A_{ap} means total
173 aperture area, $\cos(\theta_R)$ being obtained as [30]:

$$\cos(\theta_R) = \cos(\alpha_S) \times \cos(\varphi) \tag{17}$$

where φ is latitude and α_S is the angle of solar altitude given in Appendix A.

2.3. Energy analysis

The focus of the present study is not on the energy storage subsystem, but on the heliostat and receiver tower system, the steady-state analysis allowing the most relevant searched results. The energy and mass balance equations for each component of the system can be expressed as:

$$0 = \dot{m}_{in} h_{in} - \dot{m}_{out} h_{out} + \dot{Q}_{net} \quad (18)$$

$$0 = \dot{m}_{in} - \dot{m}_{out} = 0 \quad (19)$$

where h is the specific enthalpy, subscripts in and out are inlet and outlet streams of the control volume, respectively, and $\dot{Q}_{net}$ is the heat power received by the control volume, which is evaluated as:

$$\dot{Q}_{net} = \dot{Q}_S - \dot{Q}_{loss} \quad (20)$$

In the heliostat field, the solar energy input can be evaluated as [31]:

$$\dot{Q}_S = \eta_{opt} \alpha A_{ap} G_b \quad (21)$$

where A_{ap} is the total aperture area, G_b is the solar direct beam irradiation, and α is the absorption factor of the solar receiver. The thermal power losses of the system are evaluated as [32]:

$$\dot{Q}_{loss} = \dot{Q}_{loss,conv} + \dot{Q}_{loss,rad} \quad (22)$$

where subscripts conv and rad mean convection and radiation heat transfer from the solar receiver to the environment. The radiative thermal power loss can be obtained as [32]:

$$\dot{Q}_{loss,rad} = \sigma . \varepsilon_{re} . A_{re} ({T_{re}}^4 - {T_{amb}}^4) \quad (23)$$

where σ is the Stefan-Boltzman constant, ε is the receiver surface emissivity , A_{re} is the surface area of the solar receiver, and T is its absolute temperature. Subscript amb means ambient. The convective thermal power loss can be evaluated as [32]:

$$\dot{Q}_{loss,conv} = h_{forced} . A_{re} (T_{re} - T_{amb}) \quad (24)$$

A denotes the surface area of the receiver, and T its temperature. h_{forced} is the forced convection heat transfer coefficientcan be is obtained as [32]:

$$h_{forced} = \frac{k_m . Nu_{forced}}{D_{re}} \quad (25)$$

where k_m is the air thermal conductivity, and Nu and D_{re} are the Nusselt number and the solar receiver's diameter, respectively. For forced convection due to the ambient wind flow over the receiver, the Nusselt number is obtained as [32]:

$$Nu_{force} = 0.00239. Re^{0.98} + 0.000945. Re^{0.98} \quad (26)$$

the Reynolds number being evaluated as [32]:

$$Re = \frac{U_{wind} D_{re}}{\upsilon_m} \quad (27)$$

U_{wind} and υ_m mean wind speed and kinetic viscosity.

The overall ENE of the proposed system is expressed as:

$$\eta_{energy} = \frac{\dot{Q}_{net} - \dot{W}_P}{A_{ap} G_b} \quad (28)$$

where subscript p refers to the circulation pump, and $\dot{Q}_{net}$ is the net thermal power received by the receiver and $\dot{W}$ is the mechanical power needed for the circulation pump operation, evaluated as

$$\dot{W}_P = \frac{\dot{m}_1 (h_{2s} - h_1)}{\eta_P} \quad (29)$$

where h_{2s} is the specific enthalpy of the stream leaving the pump if the pumping process is assumed to be isentropic. The pump efficiency is considered 85%.

2.4. Exergy analysis

Exergy is defined as achievable mechanical work when a system reversibly evolves up to be in equilibrium with the ambient contacting it [33, 34]. Exergy analysis can be used to identify and quantify irreversibilities, and thus imperfections, in a system. For a stream, the total specific exergy is expressed as [33, 35]:

$$ex = (h - h_0) - T_0 (s - s_0) + T_0 \sum x_i R_i \ln y_i + \sum x_i ex_{chi} + \frac{V^2}{2} + gz \quad (30)$$

where T is the absolute temperature, h is the specific enthalpy, and s is the specific entropy. R_i is the particular gas constant of chemical species *i* in the stream, ex_{chi} its specific chemical exergy, x_i its mass fraction and y_i its molar fraction. g, V, and z are gravitational acceleration, velocity, , and height, respectively. Subscript 0 refers to the environmental (equilibrium) conditions. Table 1 summarizes the exergy destruction rate (EDR) relations for the main components of the system under analysis.

Table 1. EDR relations for the system main components

No.	Component	Exergy destruction rate
1	Pump	$\dot{m}(ex_1 - ex_2) + \dot{W}_P$
2	Solar receiver	$\dot{m}(ex_2 - ex_3) + \dot{Q}_{loss}\left(1 - \frac{T_{amb}}{T_{re}}\right)$
3	Heliostats	$G_b A_{ap}\left[1 - \frac{4}{3}\left(\frac{T_{amb}}{T_{Sun}}\right) + \frac{4}{3}\left(\frac{T_{amb}}{T_{Sun}}\right)^4\right] - \frac{\dot{Q}_S}{\alpha}\left(1 - \frac{T_{amb}}{T_{hel}}\right)$

The symbols and subscripts in Table 3, are defined earlier. The EXE of the proposed system can be calculated by:

$$\eta_{exergy} = \frac{\dot{Q}_{net}\left(1 - \frac{T_{amb}}{T_{re}}\right) - \dot{W}_P}{G_b A_{ap}\left[1 - \frac{4}{3}\left(\frac{T_{amb}}{T_{Sun}}\right) + \frac{4}{3}\left(\frac{T_{amb}}{T_{Sun}}\right)^4\right]} \quad (31)$$

where T_{Sun} is the Sun temperature (.

2.5. Economic analysis

Heliostat field, central tower, and receiver are the three main elements of the plant, which are analyzed separately. In what follows, the Z factors are expressed in units of US dollars. The total capital investment of the plant is evaluated as [30, 36, 37]

$$Z_{plant} = Z_{re} + Z_{tow} + Z_{piping} + Z_{heliostat\ field} \quad (32)$$

In Which, subscripts re, and tow denote receiver and tower. The investment cost of each system component is depicted in Table 2 [13, 30, 38, 39].

Table 2. The investment cost of mirrors, land, wire, and other costs

No.	Description	Cost function	Ref

1	Heliostat	Mirror	$Z_{mirror} = 126 N_{hel} A_{hel}$	[13, 30, 38, 39]
2		Wire	$Z_{wire} = \sum_{i=1}^{100} N_{hel,cell,i} \left[0.031 r_{cell,i} + 24 \sqrt{\frac{A_{hel}}{\rho_{cell,i}}} \right]$, $\rho_{cell,i} = \frac{N_{hel,cell,i} A_{hel}}{A_{cell,i}}$	[13, 30, 38, 39]
3		Land	$Z_{land} = 0.62(1.5 A_{land} + 1.8 \times 10^5)$	[13, 30, 38, 39]
4	Tower		$Z_{tow} = 1.09025 \times 10^6 \exp(0.00879 H_{tow})$ $H_{tow} < 120\ m$ $Z_{tow} = 0.78232 \times 10^6 \exp(0.01130 H_{tow})$ $H_{tow} > 120\ m$	[38, 40]
5	Piping		$Z_{piping} = \left[3600 \frac{D_{outer}}{1.31} + 420 \frac{D_{int}}{0.87} \right] H_{tow} + 90000 \frac{D_{int}}{0.87}$	[30, 36, 37]
6	Receiver		$Z_{re} = 23500 A_{re}$	[30, 36, 37]

where Z is the capital investment, D_{outer} and D_{int} are the outer and inner diameters of concentric piping. $N_{hel,cell,i}$ is the number of heliostats in cell i. $r_{cell,i}$ is the receiver - cell's center distance. Subscripts hel and land refer to heliostat and land, respectively [41]. It should be noted that the cells closer to the receiver have more heliostats; however, shorter cables are required for these cells. Wiring cost evaluation starts considering that for the cells of the equal area the density of heliostats is obtained as [13, 17, 39, 41, 42]. The cost of equipment installation is estimated as [43]

$$Z_{ins} = 0.2 Z_{plant} \tag{33}$$

Plant's maintenance costs can be estimated as [30]

$$Z_{om} = 0.03 Z_{mirror} + 0.04 Z_{tow} \tag{34}$$

Moreover, during development and building phases, some indirect additional costs must be considered, which can be estimated as [30, 44, 45]

$$Z_{if} = 0.05 Z_{plant} \tag{35}$$

Another cost related to unexpected technological/ regulatory issues is evaluated as [30, 44, 45]

$$Z_{cont} = 0.1 Z_{plant} \tag{36}$$

At the end of the heliostat field lifetime, the costs of decommissioning can be estimated as [30]:

$$Z_{dec} = 0.05 Z_{plant} \tag{37}$$

Concerning the plant operation, labor costs for 20 years of the lifetime of the project need to be considered. The salaries of the labor and required staff are presented in Table 3.

Table 3. Annual salaries and required number of staff of the plant [30]

Employee	Annual salary (US$)	Required number of staff
The operator of the control room	40000	N_{opr}
Technician of the solar field	40000	N_{tec}
Plant engineer	92000	1

In Table 3, subscripts opr and tec denote operator and technician, respectively. The number of operators for the control room can be evaluated as [30]:

$$N_{opr} = 3 + 2\left(\frac{A_{hel} N_{hel}}{100000}\right) \tag{38}$$

and the number of technicians for the solar field as [30]:

$$N_{tec} = 1 + 3\left(\frac{A_{hel} N_{hel}}{100000}\right) \tag{39}$$

Hence, the total labor cost can be expressed as [30]:

$$Z_{lab} = 1.5 \sum_{staff} sal_{stf} N_{stf} N_{years} \tag{40}$$

where N_{stf} is the number of required employees as operators, technicians, and engineers mentioned earlier. sal_{stf} is the annual salary of each employee as detailed in Table 3. N_{years} denotes the project lifetime (20 years) [31, 46]. Therefore, the total cost of the heliostat plant is obtained as:

$$Z_0 = Z_{plant} + Z_{ins} + Z_{om} + Z_{if} + Z_{cont} + Z_{dec} + Z_{lab} \tag{41}$$

The simple payback period (SPP) [31, 46]:

$$SPP = \frac{Z_0}{Z_f} \tag{42}$$

243 Z_0 is one of the most significant indices for evaluation of a plant, where Z_f is the annual income. The annual
244 cash flow Z_f can be obtained as [31, 46]:

$$Z_f = Y_{heating} k_{heating} \quad (43)$$

245 where $Y_{heating}$ is the capacity of heating production during a year, and $k_{heating}$ denotes the specific cost of
246 that heating.

247 The inflation rate effect can be evaluated by[47]:

$$Z_n = Z_0(1+i)^n \quad (44)$$

248 In which n is the number of years. i is the inflation rate which is equal to 3.11% [48]. The payback period
249 (PP) is evaluated as [31, 46]:

$$PP = \frac{\ln(\frac{Z_f}{Z_f - r.Z_0})}{\ln(1+r)} \quad (45)$$

250 where r is the discount factor (considered 3% in this study). The total gain from the plant during its lifetime
251 is defined as the net present value, evaluated as [31, 46]:

$$NPV = Z_f \frac{(1+r)^{N_{years}} - 1}{r(1+r)^{N_{years}}} - Z_0 \quad (46)$$

252 Another significant economic factor is the internal rate of return, evaluated as [31, 46]:

$$IRR = \frac{Z_f}{Z_0}\left[1 - \frac{1}{(1+IRR)^N}\right] \quad (47)$$

253
254
255 **3. MOPSO Algorithm**
256
257 The MOPSO algorithm is one kind of of the PSO algorithm to solve multi-objective optimization. The
258 MOPSO and PSO algorithms use an update of the particle location and velocity in the same manner. As it
259 is known in the PSO algorithm the update for the velocity and location of a particle can be found by
260 calculation of two parameters. These two parameters are the optimal solution that each particle is obtained
261 (individual best), and the optimal solution that the whole population is gained (global best). In the simple
262 version of the PSO algorithm, the position and speed updates can be evaluated by [49, 50]:
263

$$v_{id}(t+1) = wv_{id}(t) + r_1c_1(P_{id} - x_{id}(t)) + r_2c_2(g_d - x_{id}(t)) \quad (48)$$

$$x_{id}(t+1) = x_{id}(t) + v_{id}(t+1) \quad (49)$$

In the above equations, a and d are dimensional search space, $v_{id}(t)$, $x_{id}(t), v_{id}(t+1), x_{id}(t+1), P_{id}, g_{id}$, w, c1 and c2, and r1 and r2 are the existing particle velocity, existing particle location, newest particle velocity, newest particle location, the best result that the particle, the best result that the whole population has obtained thus far, inertia weight, acceleration coefficients, and random numbers within the interval [0,1][49, 50]. The MOPSO flowchart is represented in Figure 3.

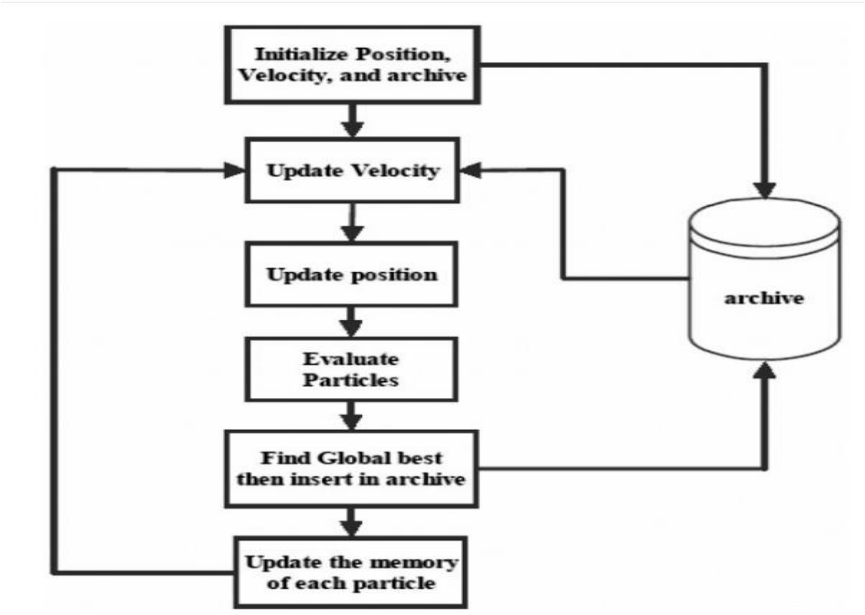

Figure 3. The flowchart of the MOPSO algorithm [51]

Two selected objective functions for the optimization are as follows:

$$\text{Objective I} = \eta_{\text{exergy}} \quad (50)$$

$$\text{Objective II} = \text{PP} \quad (51)$$

The design variables and the range of them considered in this optimization are depicted in Table 4.

277 Table 4. The ranges of design variables

No.	Design variables	Unit	Lower bond	Upper bond
1	L	m	16	25
2	l	m	6	12
3	d	m	8	14
4	H_t	m	100	140
5	β	m	5	30
6	R_a	m	2	8
7	R_H	m	8	14

278 4**. Results and discussion**

279 The outcomes of the complete 3E analyses of a typical heliostat are presented in this section. It starts
280 with validation of the model (and of its implementation in a MATLAB code) and is followed by the relevant
281 description of the location where the system is operating (Tehran City), ending with the energy, exergy, and
282 economic results and analysis. For that purpose, it is assumed that all the thermal energy reaching the
283 storage tank in Fig. 1 is used daily. In the first step, the solar radiation in each hour is calculated through a
284 year. After it, the amount of solar radiation absorbed by the solar receiver is calculated. Then, considering
285 the energy analysis the outlet temperature of the storage tank is calculated. By calculating the
286 thermodynamic properties in each stream of the system, the exergy evaluation is done. By considering the
287 initial and installation cost and other indirect costs, the economic investigation is done. For the optimization,
288 the two target functions are considered and the Pareto-front figure is presented and the optimization point
289 is selected. For the parametric study, the results of the heliostat field are compared before and after
290 optimization. Input parameters of the heliostat field model are summarized in Table 5 [9, 13, 26, 41, 52-
291 54]. Properties of the working fluid(Therminol VP-1), are tabulated in Table 6 [55].

292
293
294

295 Table 5. Input parameters of the model

No.	Parameter	Unit	Value/definition
1	Working fluid	-	Therminol VP-I
2	L	m	20
3	H_t	m	120
4	d	m	10
5	R_a	m	4
6	R_H	m	9
7	L_H	m	12.3
8	L_W	m	9.8
9	Field zones number	-	3
10	N_{hel}	-	20
11	N_{tot}	-	1460
12	φ	Degree	35.689 N
13	L_{loc}	Degree	51.5 E
14	Field layout	-	Radial-staggered/spired
15	l	m	8
16	The additional separation distance between adjacent heliostats	m	0
17	$\dot{m}$	kg/s	4.5
18	β	Degree	10
19	Heliostat vertical distance from the ground	m	5
20	P_1	kPa	101.3

296 Table 6. Properties of Therminol VP-1 [55]

297

No.	Parameter	Unit	Value/definition
1	Composition	-	Biphenyl/diphenyl oxide eutectic mixture

2	Density at 15℃	kg/m^3	1069
3	Thermal conductivity at 15 ℃	W/(mK)	0.1367
4	Specific heat at 15 ℃	kJ/(kgK)	1.529
5	Viscosity at 15 ℃	kg/(ms)	0.005051
6	Specific enthalpy at 15 ℃	kJ/kg	4.7
7	Normal boiling point	℃	257
8	Crystallizing point	℃	12
9	Average molecular weight	kg/kmol	166
10	Maximum bulk temperature	℃	400
11	Flashpoint PMCC	℃	110
12	Flashpoint COC	℃	124

4.1. Model validation

Results from Ref [39] were used for the model validation. The model was implemented in MATLAB, and the data summarized in Table 6 from Ref [39] inserted in the developed code. The comparison between the key parameters of the heliostat solar tower evaluated using the present model (and its implementation) with the data in Table 20 of Ref [39] is made in Table 7. For evaluation of the EXE of the heliostat system, the reference [56] is considered. In that reference, the solar radiation about 800 W/m^2 and heliostat and central receiver characteristics in Table 1 of that reference are considered. The heliostat field and central receiver EXE's are calculated about 75.0% and 55.8%, respectively in that reference. So, in general, the EXE of the total heliostat system is about 41% by multiplying these two exergy efficiencies. By inserting the solar radiation and heliostat and central receiver of the reference [56], the total EXE is calculated around 38.9%. The deviation is around 5% which is acceptable in engineering calculation.

Table 7. Comparison of results of the present model and Ref [39]

No.	Parameter	Unit	Model	Ref [39]	Difference (%)
1	Annual thermal energy provided by the heliostat field	GWh	102.3	99.275	3
2	Heliostat field mean cosine efficiency	%	85.1	83.21	2.2
3	Heliostat field mean attenuation efficiency	%	94.1	95.23	1.2
4	Heliostat field averaged spillage efficiency	%	94	97.68	4

4.2. Heliostat location

The field is located in Tehran City, Iran, at 35.41° N latitude and 51.19° E longitude [57]. Tehran City is a semi-arid metropolis with very hot summers and cold winters, with eventual snowfall. Based on a yearly average, Tehran City has about 13 daylight hours and 11 hours of sunshine[58, 59][59, 60][59, 60. As can be seen from Figure 4, the city experiences the maximum and minimum temperatures in July and in January, respectively. The three months with the highest temperatures (by decreasing order) are July, August, and June, and the three months with the lowest temperatures (by increasing order) are January, February, and December. The mean temperature changes from 3.8 ℃ up to 21.8 ℃. Generally, the highest temperature in the city is 36.9 ℃, and the lowest temperature is 0.3 ℃ [60].

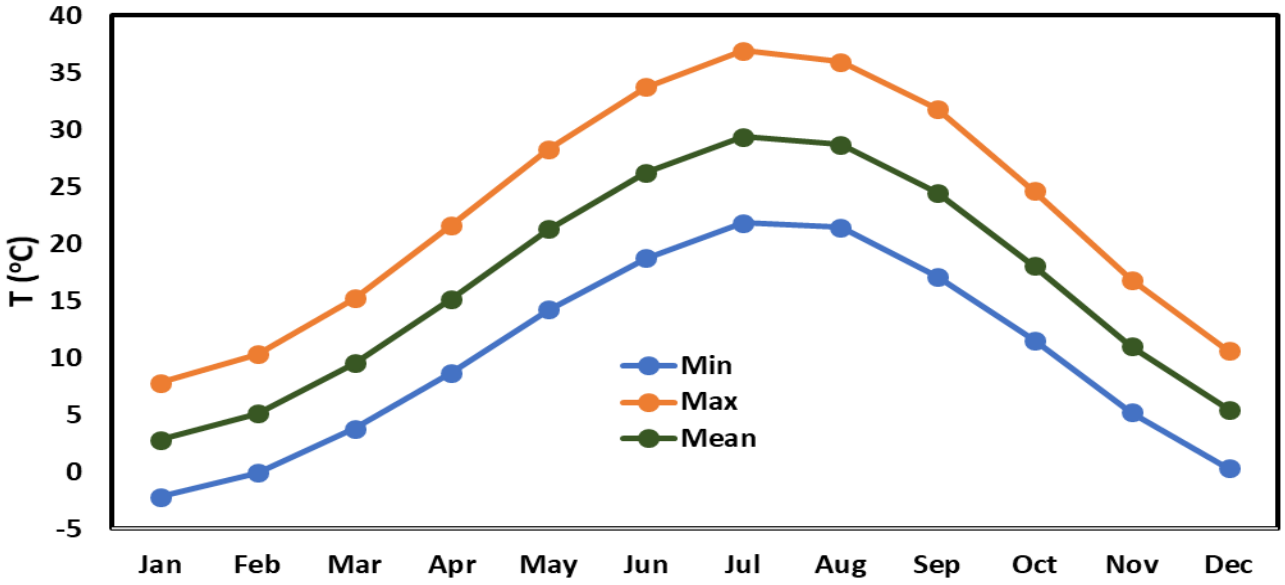

Figure 4. The minimum, maximum, and mean temperatures of the Tehran City

Table 8 summarizes detailed information about annual wind speed in Tehran, categorized by different wind velocity ranges. The annual total amount of wind velocity for each range also can be found. This number means the total number of occurrences of wind flow within each of the wind velocity range along a year. Figure 5 reports the mean wind velocity of Tehran City during a year. As illustrated, the maximum mean wind velocity of about 5.9 m/s occurs in May, and December has the lowest mean wind velocity of about 3.6 m/s. The three months of April, May, and June have the highest mean wind velocities, and August, September, and December have the minimum mean wind velocities.

Table 8. The quantity of wind velocity in the particular ranges for each month in Tehran [61-63]

Wind velocity	Jan	Feb	Mar	Apr	May	Jun	Jul	Aug	Sep	Oct	Nov	Dec	Annual
$1 \leq U_{wind}$	59	62	82	79	71	76	98	106	119	96	64	60	752
$4 \leq U_{wind}$	25	36	65	61	53	67	73	51	43	37	31	8	473
$7 \leq U_{wind}$	15	22	20	32	27	27	7	5	6	10	14	2	161
$11 \leq U_{wind}$	0	2	2	7	12	3	2	1	0	2	2	2	29
$U_{wind} > 16$	0	0	0	0	0	0	0	0	0	0	0	0	0

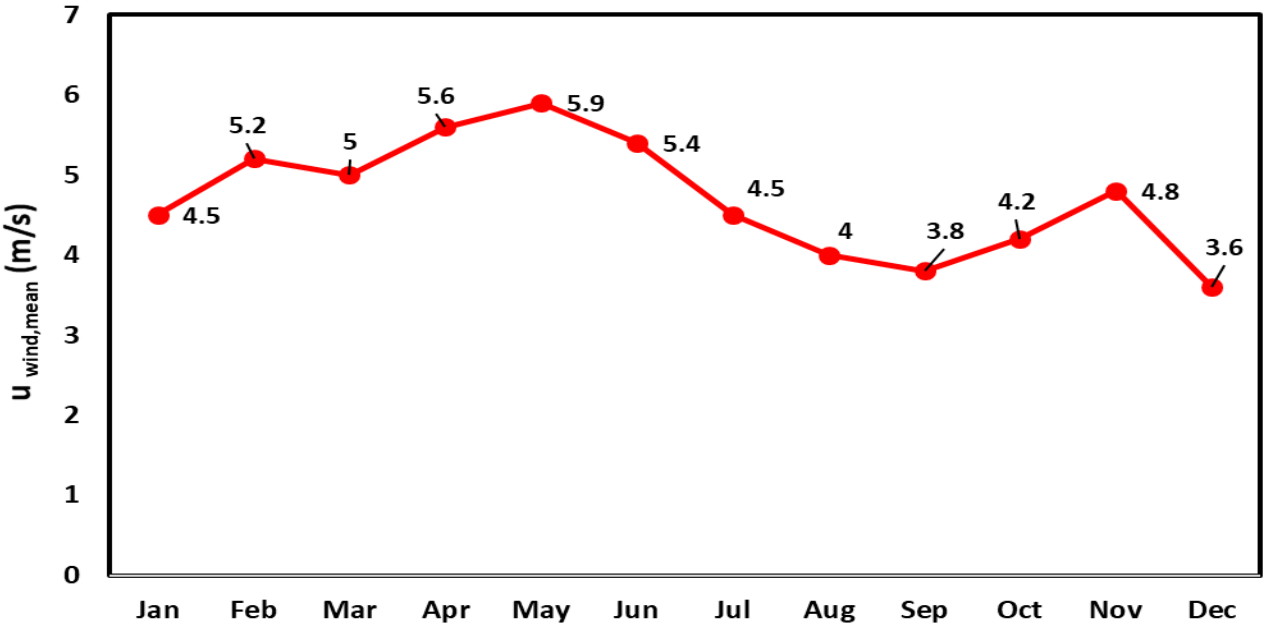

Figure 5. Mean wind velocity in the Tehran City

Figure 6 presents the solar radiation during January, May, and July 15th. As can be seen, the solar radiations for July and May are close, with a maximum close to 894 W/m^2. The highest achievable solar radiation in January is about 641 W/m^2. Since January has a late sunrise and early sunset in comparison to May and July, the solar radiation is significantly lower. A typical day of May and July has 13 and 14 hours of solar radiation, respectively.

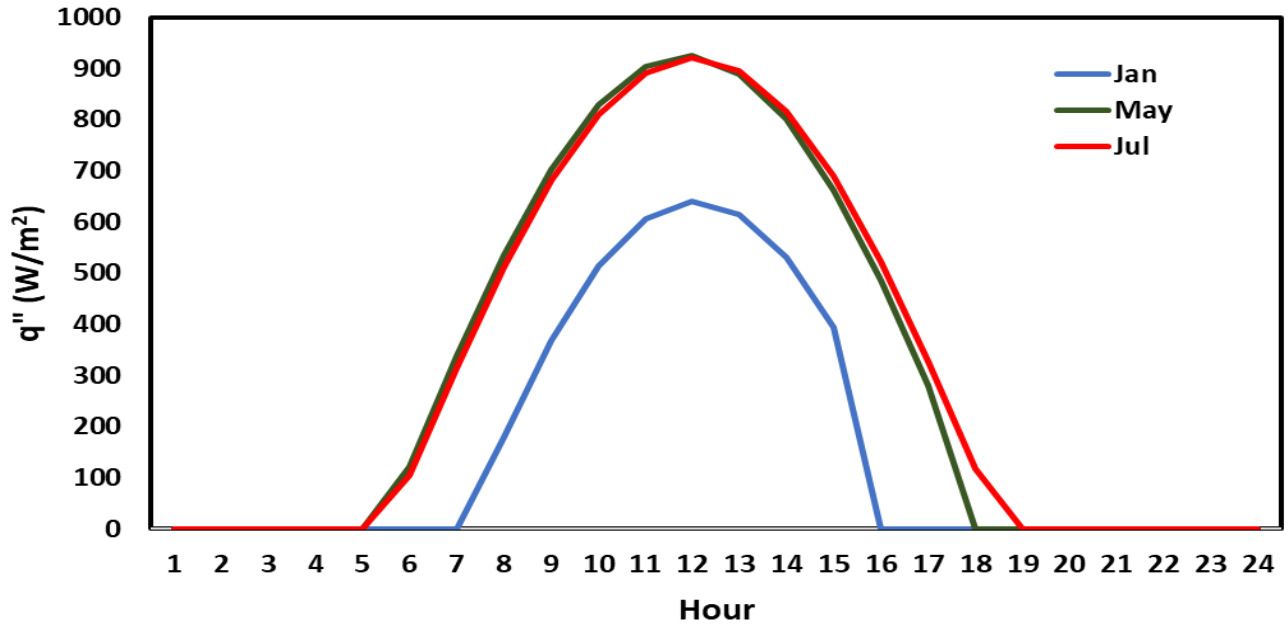

Figure **6.** Solar radiation during the January, May, and July 15th

4.3. Daily energy analysis of the heliostat field

Figure 7 presents the absorbed solar power by the solar receiver, $\dot{Q}_{abs}$ being the absorbed solar radiation from the heliostats to the solar dish. As depicted, the maximum absorbed solar power of about 70.9 MW belongs to July, followed by 68.1 MW maximum solar power absorbed in May. Similarly, to Figure 5, January has the lowest maximum absorbed solar power of about 45.6 MW.

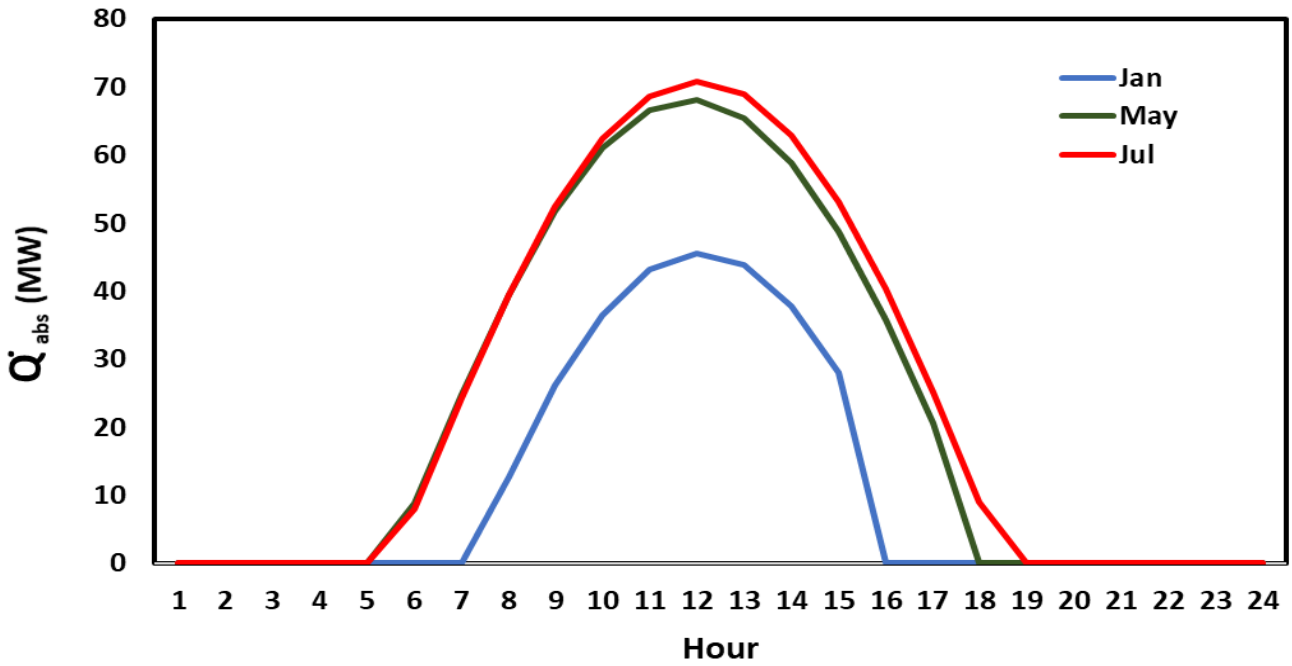

Figure 7. Absorbed solar power without any losses during January, May, and July 15th

Figure 8 presents the solar receiver outlet temperature for January, May, and July 15th. For all these three months, this temperature increases when the sun rises, but with different behaviors for each month. The decrease of this outlet temperature begins with the sunset, as no more solar radiation is available and thermal energy losses from the solar receiver become dominant. Although May and July trends are close to each other, the highest outlet temperature of about 490 ℃ occurs in July. The highest achievable solar receiver outlet temperature for May is about 465 ℃, the lowest outlet temperature of about 259 ℃ belonging to January.

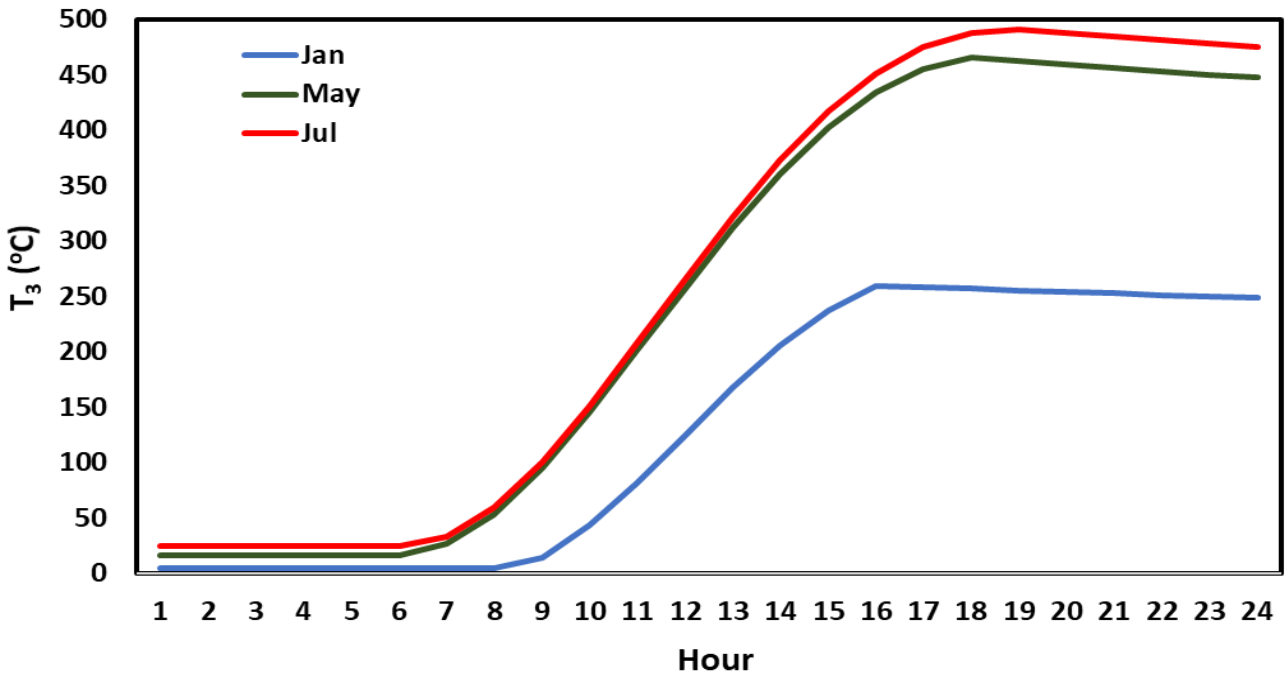

Figure 8. Outlet temperature from the solar receiver during January, May, and July 15th

4.4. Optimization results

Figure 9 shows the Pareto-front curve for variation of objective functions versus decision variables depicted in Table 4. In this figure, the effects of changing the decision variables on objective functions are presented. In the optimized point, the EXE reaches 38.9% and the PP is reduced to 4.3 years. Table 9 shows the optimized decision variables.

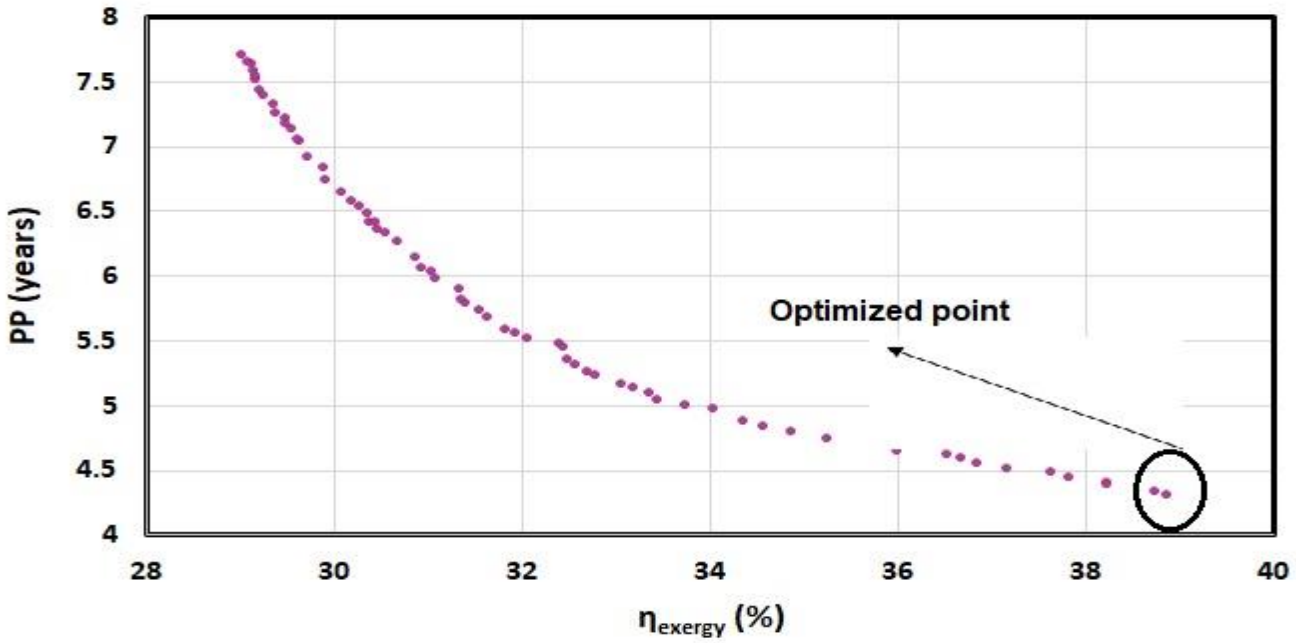

359

360 Figure 9. The Pareto-front curve

361 Table 9. The optimized decision variables

No.	Design variables	Unit	Optimized value
1	L	m	17.1
2	l	m	6
3	d	m	8.1
4	H_t	m	100.5
5	β	m	6
6	R_a	m	2
7	R_H	m	8

362

363

4.5. Parametric study

Figure 10 displays the monthly average heliostat optic efficiency before and after optimization. The maximum optic efficiency of about 56.7% belongs to July, December having the lowest heliostat optic efficiency of about 47.5 %. While after optimization, these values reach 59.5% and 49.2%, respectively. It is noticeable that the variation between the minimum and maximum achievable heliostat optic efficiency over a year is not significant. Moreover, the highest heliostat optic efficiency can be obtained in the four months of April, May, June, and July.

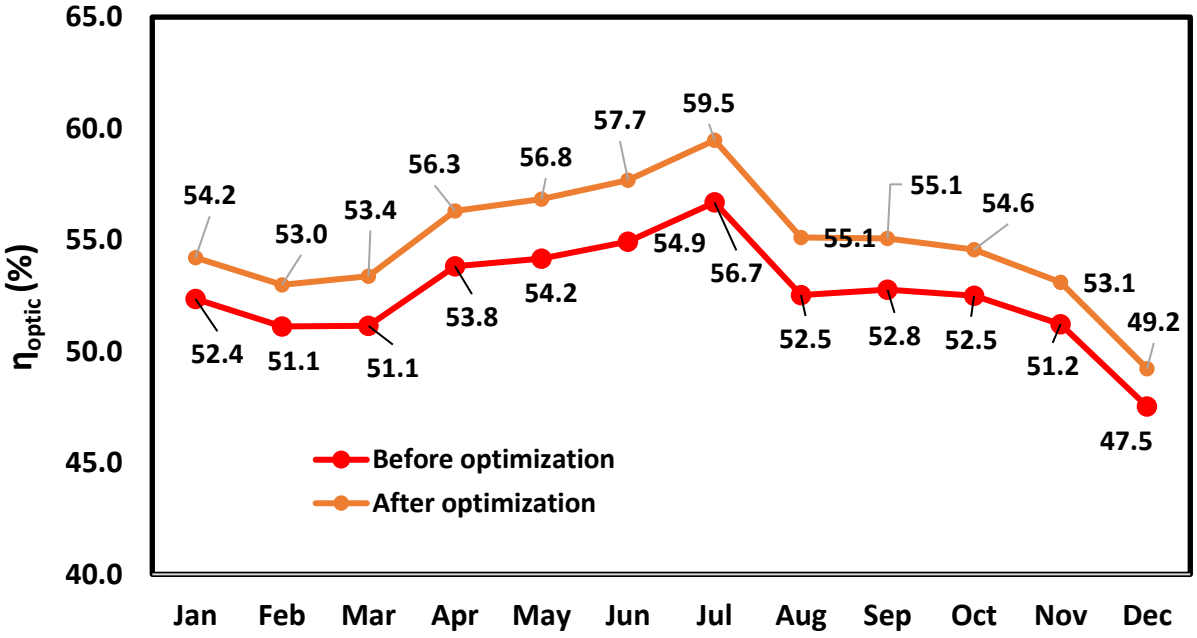

Figure 10. Monthly average of the heliostat optic efficiency before/after optimization

Figure 11 presents the monthly averaged absorbed solar energy for each month before/after optimization. As mentioned before, the Q_{abs} defines solar energy absorbed without any loss. The highest achievable absorbed solar power is about 2.6 TJ which occurs in July, December having the lowest of about 1.1 TJ. The three months of November, December, and January have a low potential for solar energy absorption; on the opposite side, May, June, and July have the highest potential for solar energy absorption. Several reasons can be invoked for lower absorbed solar power in December than in January, such as the heliostat optic efficiency and angle of radiation. By doing optimization, the average solar energy absorbed is improved. This increase is more considerable in hot months than cold ones.

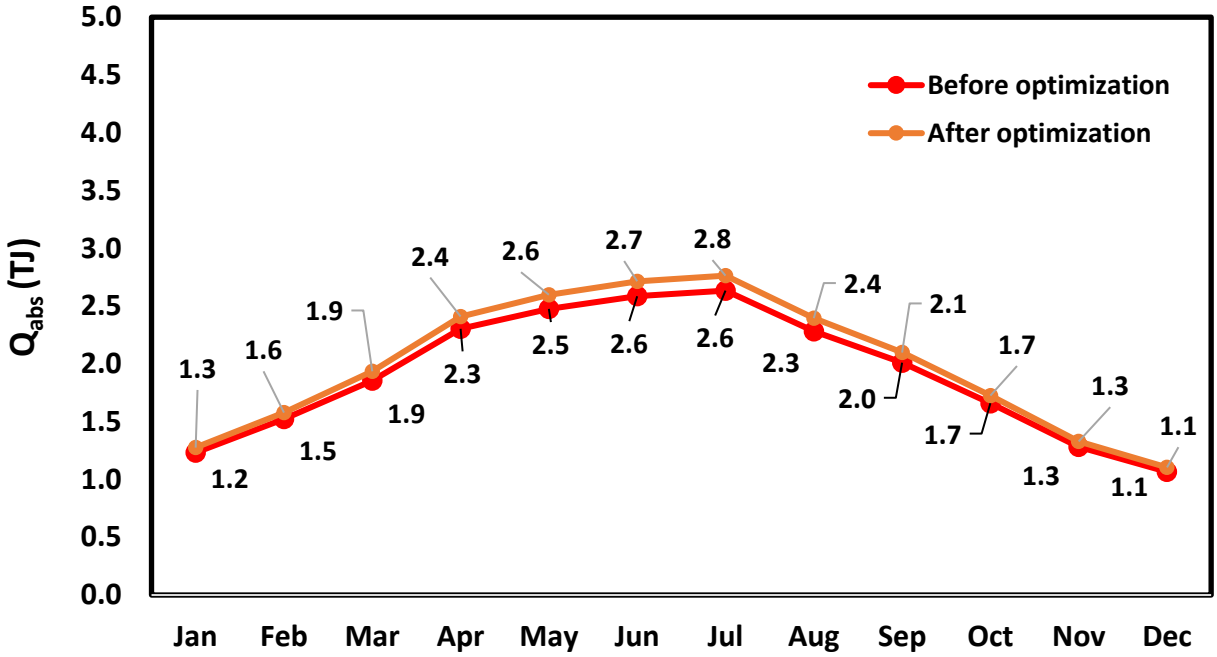

Figure 11. Monthly average absorbed solar energy

Figure 12 exhibits the monthly averaged outlet temperature from the solar receiver for each month before/after optimization. As can be seen, this means temperature reaches a maximum of 274.9 ℃ in July and a minimum of about 123.6 ℃ in December before optimization. The highest mean working fluid temperatures occur in May, Jun, and July, November, December, and January having the lowest mean working fluid temperatures. Optimization of the heliostat field improves the outlet temperature of the working fluid. For example, in July the working temperature reaches 322.2 ℃ (around 17.2%).

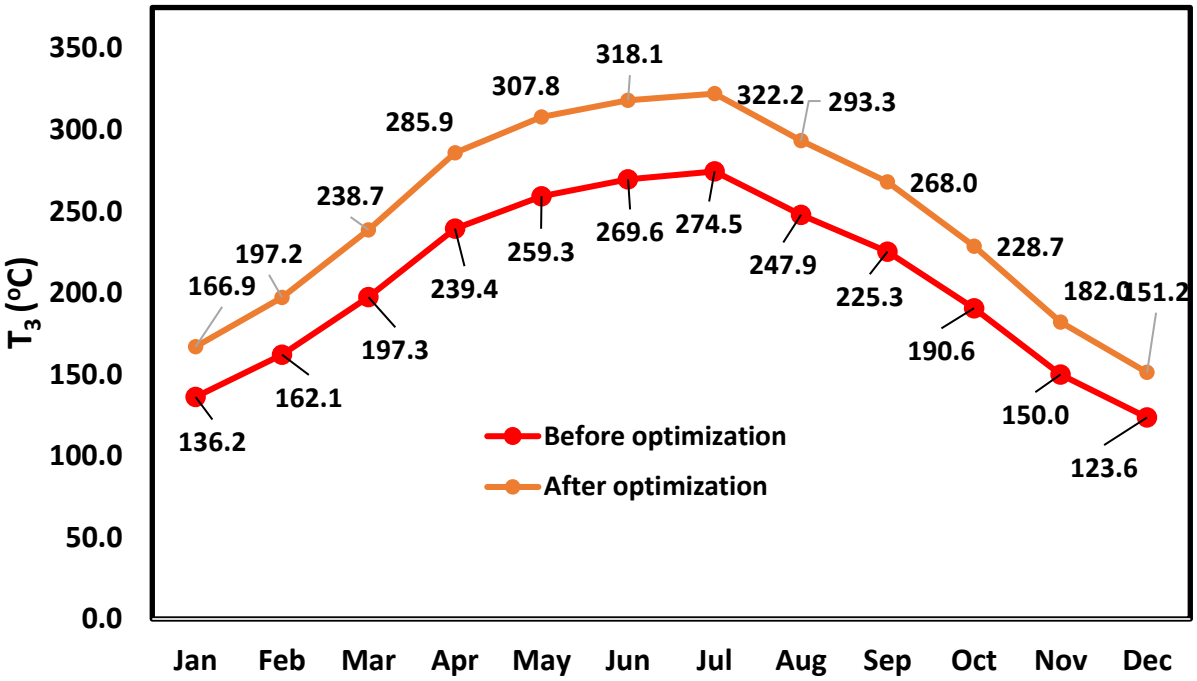

Figure 12. Monthly average outlet temperature from the solar receiver

Figure 13 illustrates the monthly average heliostat solar tower ENE before and after optimization. Similar to previously presented results, the maximum ENE of about 49.4% belongs to July, December having the lowest ENE of about 42.6%. Although there is a significant difference in the average net energy absorbed by the solar tower in the July and December months, as depicted in Figure 11, there is a comparatively slight difference of about 16% on the ENE's. This is due to the solar energy input in the denominator of Eq. (28). As the solar energy input for each month changes, and is at the lowest level in months such as December and January, the reduction of both the numerator and the denominator for these months decreases the corresponding ENE's difference. After optimization, the ENE is improved. For example, in July, the heliostat field ENE is improved from 49.4% to 53.8%.

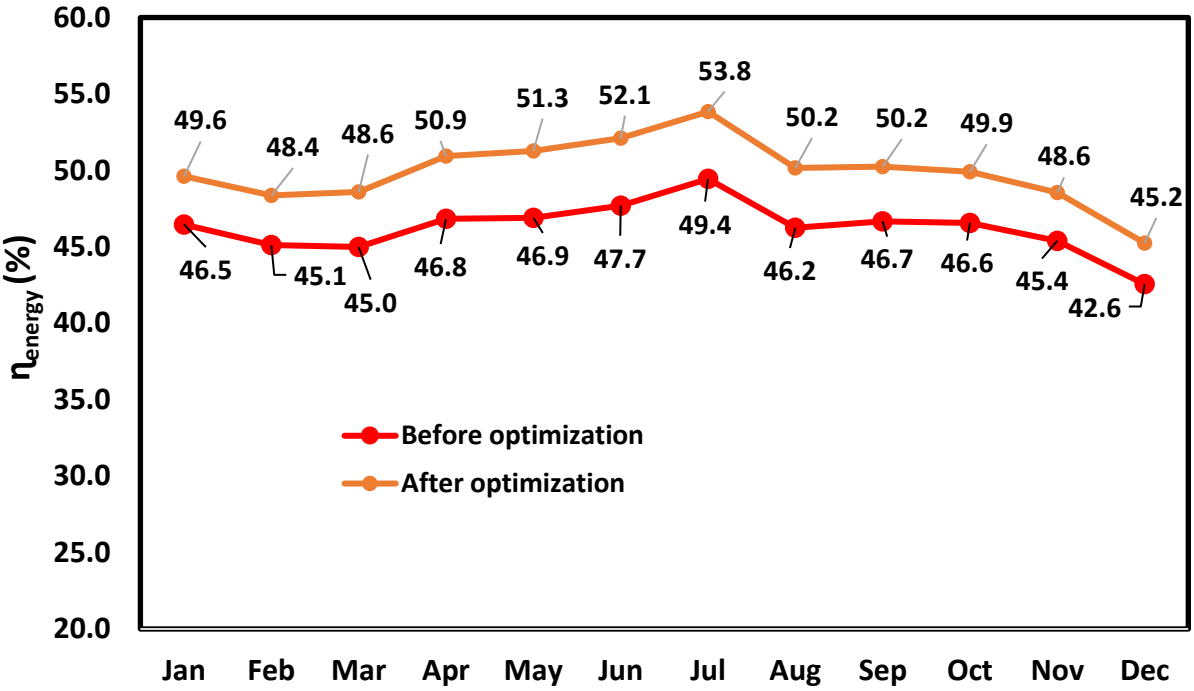

Figure 13. Monthly average heliostat solar tower ENE

Figure 14 shows the monthly averaged heliostat solar tower EXE The trends in Figures 13 and 14 are similar. July has the highest EXE of about 34.7%, and December the lowest EXE of about 26.2%. The highest EXE is available in the three months of May, June, and July. Since both energy and EXE's follow the same pattern and only the numerator and denominator of EXE are multiplied with a ratio. Similar to the heliostat field ENE, the heliostat field EXE is promoted.

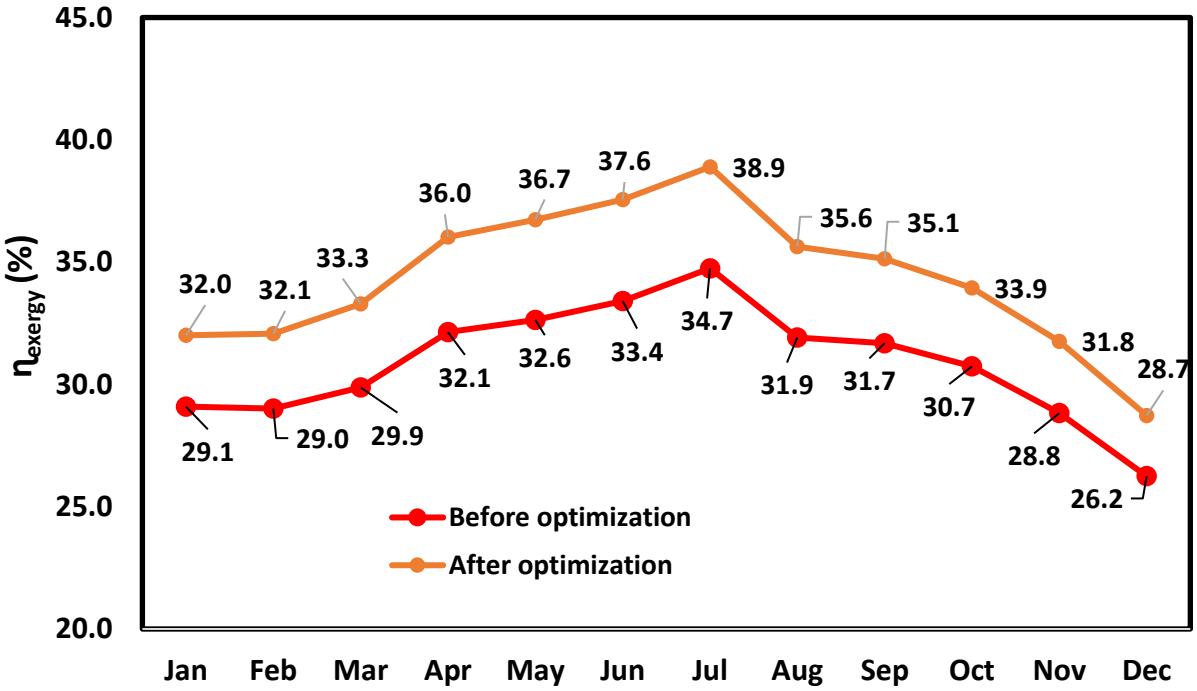

Figure 14. Monthly averaged heliostat solar tower EXE during a year

Figure 15 shows the annual ENE and EXE of the heliostat solar field before and after optimization., These values before optimization are equal to 46.2% and 30.9%, respectively while the MOPSO optimization algorithm improves these values to 49.9% and 34.4%, respectively.

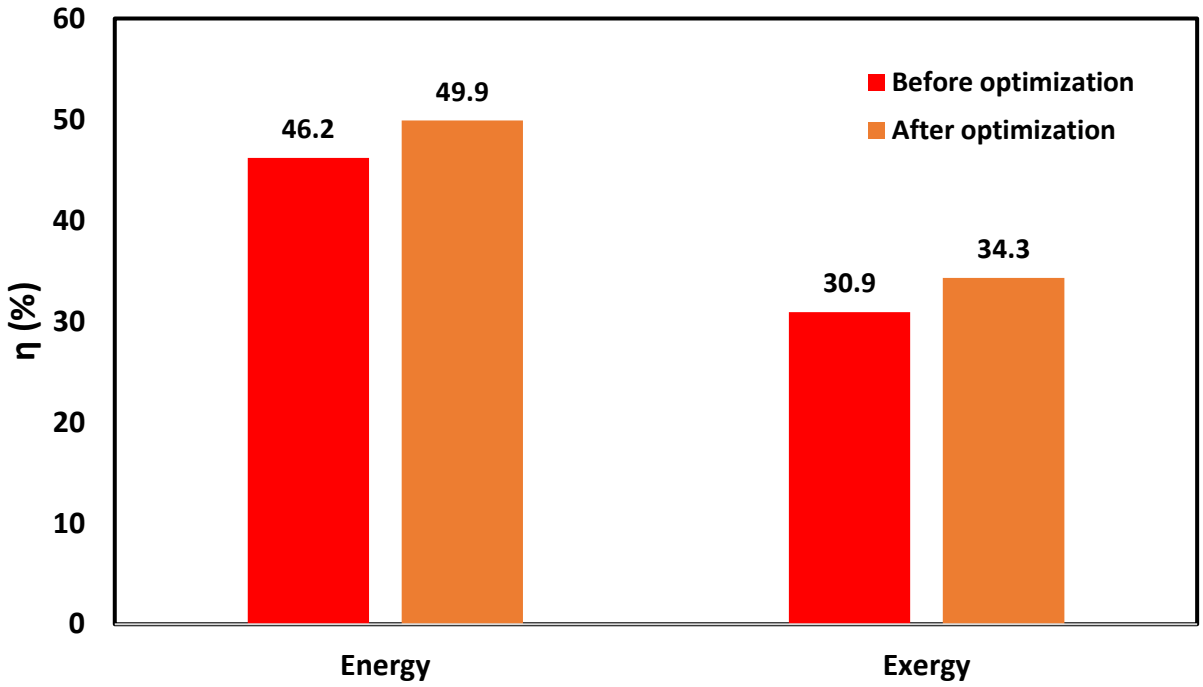

Figure 15. The annual ENE and EXE of heliostat solar tower

The results of the economic evaluation and annual ENE and EXE of the heliostat solar tower are summarized in Table 10.

Table 10. Economic results of the heliostat solar field

No.	Parameter	Unit	Value (Before optimization)	Value (After optimization)
1	NPV	US$	58.84×10^6	63.34×10^6
2	SPP	Year	6.04	3.8
3	PP	Year	6.76	4.3
4	IRR	–	0.16	0.19

From Table 10 it can be concluded that the PP is of 6.76 years, which is slightly higher than SPP. Considering the expected lifetime of 20 years for the system, this indicates the economic viability of the system, not far from that of many other systems for renewable energy capture and conversion. The IRR and NPV are equal to 0.16, and 58.84×10^6 US$, respectively. Like in all renewable energy systems, it must be emphasized that the real economic results will depend also on the environmental conditions, the most important environmental condition for solar-powered systems being solar radiation. By using the

MOPSO algorithm, the PP and SPP are reduced to 4.3 and 3.8 years, respectively. Also, the NPV and IRR are increased to 63.34×10^{6} and 0.19, respectively.

5. Conclusions

A lot of research has been made in the subject of heliostat solar field integrated with other systems to produce electricity, heating, and cooling. However, no significant research has been conducted concerning the single heliostat solar field, and especially its energy, exergy, and economic analyses. Also, optimization of this field has not been done before. The model of the heliostat field includes a lot of related geometric information leading to the optic characteristics and efficiency of these systems. The whole system energy and exergy performance depends also on the profile of the thermal energy storage, depending on the solar energy capture and the thermal energy use, this depending on the energy use profile. As the focus is on the heliostat system receiver, it is assumed that the net thermal energy is consumed at the same rate as it is captured. The model for evaluation of the energy and exergy performances of these systems includes also the location and environment conditions, a good performance being obtained with the properly designed equipment and operation together with the expected environmental conditions. The economic input data are of major relevance for the evaluation of the economic system's viability; however, they are only estimating, that can experience considerable unpredictable changes during the system's lifetime due to reduction in performance caused by depreciation. MOPSO optimization algorithm is carried out for 7 parameters of the heliostat field. Two objective functions including EXE and payback period are considered for this optimization. Once the model and its imp mentation were validated by comparison with information obtained from the literature, it was for the specific system under analysis when operating in Tehran City. Detailed yearly environment data from Tehran City, with emphasis on the available solar radiation, allows anticipation of the best periods of the system's operation. Results show that the heliostat optical efficiency presents only slight changes during a year, being maximum in July and minimum in December, and having a yearly average value slightly above 50%. The monthly averaged absorbed solar power, the monthly averaged outlet temperature from the solar receiver, and the monthly averaged net energy absorbed by the solar receiver follow essentially similar patterns along a year, strongly dictated by the net heat received in each month, with maximum value in July and minimum value in December. The monthly averaged solar ENE of the solar tower changes slightly during a year, with a maximum value in July (49.4%) and minimum value in December (42.6%), with an average value close to 46%. The monthly averaged solar exergy efficiency of the heliostat presents more changes than the monthly averaged solar ENE along a year, by the maximum in July (34.7%) and minimum in December (26.2%), with an average value close to 31%. From economic analysis are highlighted a PP is of 6.76 years, slightly higher than the SPP of 6.04 years. These are not far from that of many other systems for renewable energy capture and conversion, indicating the economic viability of the system considering its expected lifetime operation for 20 years. The results of the optimization reveal that the annual average energy rose to 49.9% and the EXE increase to 34.3. Also, the payback period of the heliostat field decrease from 6.76 to 4.3 years.

477

478 **Nomenclature**

Acronyms:

CSP	Concentrated solar power
ENE	Energy efficiency
EXE	Exergy efficiency
GA	Genetic algorithm
IRR	Internal Rate of Return
LCoE	Levelised Cost of Electricity
MOPSO	Multi-Objective Particle Swarm Optimization
NPV	Net Positive Value
PP	Payback Period
PSO	Particle Swarm Optimization
SPP	Simple Payback Period

Symbols:

A, B	Constant in equation (5)
A_{ap}	Total aperture area (m^2)
$A_{cell,i}$	Area of cell i (m^2)
A_{hel}	Area of one heliostat (m^2)
A_{land}	Heliostat field land area (m^2)
A_{re}	Solar receiver area (m^2)
d	Heliostat - receiver distance (m)
D	Reflected area diameter (m)
D_{re}	Receiver's diameter (m)
desp	Extra separation between adjacent heliostats (m)
DM	Distance between adjacent heliostats centers (m)
ex	Specific exergy (J/kg)
g	Gravitational acceleration (m/s^2)

G_b	Direct normal irradiance (W/m^2)
h	Specific enthalpy (J/kg)
H	Height (m)
h_{forced}	Forced convection heat transfer coefficient (W/(m^{2}K))
h_S	Angle of the solar hour (degrees)
k_m	Thermal conductivity (W/(m.K))
l	Reflector length (m)
L	Height of absorbing area (m)
L_H	Heliostat height (m)
L_W	Heliostat width (m)
L_{loc}	Location longitude (degrees)
L_{st}	Local standard meridian (degrees)
$\dot{m}$	Mass flow rate (kg/s)
N	Number of days of a year in equation (20)
Nu	Nusselt number
N_{hel}	Total number of heliostats
$Nhel_1$	The number of first zone heliostats in every line
$N_{hel,cell,i}$	The heliostats' number in cell i
$Nrow_i$	The number of heliostats rows
$\dot{Q}$	Heat transfer rate (W)
r	Discount factor
R	Distance between each heliostat and the base of the tower (m)
R	Specific gas constant (J/kg.K)
R_a	Receiver radius (m)
R_H	Receiver height (m)
r_{ap}	Effective size of receiver opening (m)
$r_{cell,i}$	Distance of the receiver and the cell center (m)
R_i	Radial distance between the first row of ith field and the tower (m)
r_{int}	Inner radius of the concentric piping (m)

r_{outer}	Outer radius of the concentric piping (m)
Re	Reynolds number
s	Specific entropy (J/kg.K)
T	Temperature (K)
U_{wind}	Wind velocity (m/s)
V	Velocity (m/s)
$\dot{W}$	Work rate (W)
x_i	Mass fraction of component i
y_i	Molar fraction of component i
z	Height (m)
z_0	Investment cost (US$)
Z_{cont}	Additional funding required for unexpected technological and regulatory issues (US$)
z_f	Annual cash flow (US$)
Z_i	Capital investment of component i (US$)

Greek symbols:

α	Absorption angle of the solar receiver (degrees)
β	Parameter in equation (2)
β_{hs}	Angle of rotation of incident solar radiation (degrees)
δ	Deflection angle (degrees)
δ_S	Solar declination (degrees)
ε	Emissivity of a surface
ε_{surf}	Errors caused by angular deviation
ε_{track}	Errors caused by tracking
η	Efficiency
θ_R	Angle of received reflected irradiation from heliostat field (degrees)
θ_S	Angle of solar incidence (degrees)
θ_z	Angle of solar zenith (degrees)
λ_s	Angle between vertical direction and reflected irradiation (degrees)

$\rho_{cell,i}$	Density of heliostats in cell i
σ	Constant of Stefan-Boltzmann ($W/m^2.K^4$)
σ_1	Parameter in equation (34)
α_S	Angle of solar altitude (degrees)
φ	Latitude angle (degrees)
φ'	Solar azimuth angle (degrees)
φ_S	Angle of solar azimuth (degrees)
ω	Sunset hour angle (degrees)
Δaz_1	Azimuth angular spacing (degrees)
ΔR_{min}	Minimum radial increase of the field (m)

Subscripts:

0	environment condition
abs	absorbed
amb	ambient
at	atmospheric attenuation
ch	chemical
conv	convection
cos	cosine
dec	decommissioning
hel	heliostat
i	line i of the field
if	indirect factors
in	inlet stream
Ins	installation
lab	labor
lat	latitude
min	minimum
om	operation and maintenance
opr	operator

opt	optic
out	outlet stream
p	pump
rad	radiation
re	receiver
ref	rate of mirror reflectivity
S	sun
s&b	shadowing and blocking
surf	surface
tec	technician
T	tower

Appendix A. Solar radiation modeling

The solar time is evaluated as [64-66]:

$$\text{Solar time} = \text{Standard time} + \mathrm{E} - 4(\mathrm{L_{st}} - \mathrm{L_{loc}}) \quad \text{(A.1)}$$

where $\mathrm{L_{loc}}$ is the location longitude, $\mathrm{L_{st}}$ is the local zone time standard meridian, and E is obtained as [64-66]

$$\mathrm{E} = 229.2(0.000075 + 0.001868\mathrm{Cos}\beta - 0.04089\mathrm{Sin}2\beta - 0.014615\mathrm{Cos}2\beta - 0.032077\mathrm{Sin}\beta) \quad \text{(A.2)}$$

In Eq. (2) β is equal to $\frac{(\mathrm{n}-1)360}{365}$, where for January first *n* is equal to 1. The sunset hour angle is evaluated as [64-66]

$$\omega = \arccos(\tan(\varphi)\tan(\delta)) \quad \text{(A.3)}$$

where δ denotes the angle of deflection and φ the location latitude. The angle of deflection δ can be evaluated as [25]

$$\delta = 23.45\sin\left(\frac{360(284+\mathrm{n})}{365}\right) \quad \text{(A.4)}$$

The direct normal irradiance $\mathrm{G_b}$ is obtained as [25]

$$G_b = A\cos(\theta_z)\exp\left(\frac{-B}{\cos(\theta_z)}\right) \quad \text{(A.5)}$$

where θ_z denotes the angle of solar zenith, and A and B are constants adapted from Ref [25]. These constants are based on the average metrological data during 10 years. The angle of solar zenith can be evaluated as [67]

$$\theta_z = 90° - \alpha_S \quad \text{(A.6)}$$

where the $\boldsymbol{\alpha_S}$ is the solar altitude angle.

The angle of solar altitude is obtained as follows [68]:

$$\alpha_S = \sin^{-1}[\sin(\phi\ ).\sin(\delta_S) + \cos(h_S).\cos(\phi\ ).\cos(\delta_S)] \quad \text{(A.7)}$$

The angle of the solar hour can be expressed as [67]:

$$h_S = 15° \times (\text{Solar time} - 12) \quad \text{(A.8)}$$

where solar time defines the time that the sun was shining for a day.

The solar azimuth angle can be obtained as [55]

$$\varphi' = \sin^{-1}\left(\frac{\sin(h_S).\cos(\delta_S)}{\sin(\theta_z)}\right) \quad \text{(A.9)}$$

where θ_z is the angle of solar zenith. The conditions for the angle of the solar hour can be expressed as follows [55]:

$$\text{If} \quad \cos(h_S) \geq \left(\frac{\tan(\delta_S)}{\tan(\phi_{lat})}\right), \qquad \varphi_S = 180° - \varphi' \quad \text{(A.10)}$$

$$\text{else} \quad \varphi_S = 180° + \varphi' \quad \text{(A.11)}$$

where φ_S is the angle of surface azimuth.

The angle of surface azimuth is evaluated as [55]:

$$\text{If} \quad \varphi_S - \varphi' > 0, \qquad \varphi_{surf} = \varphi' + 90° \quad \text{(A.12)}$$

$$\text{else} \quad \varphi_{\text{surf}} = \varphi' - 90° \tag{A.13}$$

where subscript surf means surface.

Funding: There is no financial support provided by any specific governmental and institutional organization to complete this manuscript.

Conflict of Interest: The authors declare that they have no conflict of interest.

References

[1] Alizadeh S, Ghazanfari A, Ehyaei M, Ahmadi A, Jamali D, Nedaei N, et al. Investigation the integration of heliostat solar receiver to gas and combined cycles by energy, exergy, and economic point of views. Applied Sciences. 2020;10(15):5307.

[2] Gielen D. Renewable energy technologies: Cost analysis series-Concentrating Solar Power. 2012. International Renewable Energy Agency: Bonn, Germany.

[3] Ahmadi A, Ehyaei MA, Jamali DH, Despotovic M, Esmaeilion F, Abdalisousan A, et al. Energy, exergy, and economic analyses of integration of heliostat solar receiver to gas and air bottom cycles. Journal of Cleaner Production. 2021;280:124322.

[4] Gupta M, Kaushik S, Ranjan K, Panwar N, Reddy VS, Tyagi S. Thermodynamic performance evaluation of solar and other thermal power generation systems: A review. Renewable and Sustainable Energy Reviews. 2015;50:567-82.

[5] Hachicha AA, Yousef BA, Said Z, Rodríguez I. A review study on the modeling of high-temperature solar thermal collector systems. Renewable and Sustainable Energy Reviews. 2019;112:280-98.

[6] Dowling AW, Zheng T, Zavala VM. Economic assessment of concentrated solar power technologies: A review. Renewable and Sustainable Energy Reviews. 2017;72:1019-32.

[7] Rajendran DR, Sundaram EG, Jawahar P, Sivakumar V, Mahian O, Bellos E. Review on influencing parameters in the performance of concentrated solar power collector based on materials, heat transfer fluids and design. Journal of Thermal Analysis and Calorimetry. 2020;140(1):33-51.

[8] Eddhibi F, Amara MB, Balghouthi M, Guizani A. Optical study of solar tower power plants. Conference Optical study of solar tower power plants, vol. 596. IOP Publishing, p. 012018.

[9] Noone CJ, Torrilhon M, Mitsos A. Heliostat field optimization: A new computationally efficient model and biomimetic layout. Solar Energy. 2012;86(2):792-803.

[10] Atif M, Al-Sulaiman FA. Optimization of heliostat field layout in solar central receiver systems on annual basis using differential evolution algorithm. Energy Conversion and Management. 2015;95:1-9.

[11] Talebizadeh P, Mehrabian MA, Rahimzadeh H. Optimization of heliostat layout in central receiver solar power plants. Journal of Energy Engineering. 2014;140(4):04014005.

[12] Li C, Zhai R, Yang Y. Optimization of a heliostat field layout on annual basis using a hybrid algorithm combining particle swarm optimization algorithm and genetic algorithm. Energies. 2017;10(11):1924.

[13] Saghafifar M. Thermo-economic optimization of hybrid combined power cycles using heliostat field collector 2016.

[14] Zi WXLZL, Zhifeng W. Design and Optimization of Heliostat Field Layout for Solar Tower Power Plant [J]. Acta Optica Sinica. 2010;9.

[15] Toro C, Rocco MV, Colombo E. Exergy and thermoeconomic analyses of central receiver concentrated solar plants using air as heat transfer fluid. Energies. 2016;9(11):885.

[16] Zhang M, Yang L, Xu C, Du X. An efficient code to optimize the heliostat field and comparisons between the biomimetic spiral and staggered layout. Renewable Energy. 2016;87:720-30.

[17] Saghafifar M, Gadalla M. Improvement in spiral heliostat field layout thermo-economic performance by field zoning implementation. Conference Improvement in spiral heliostat field layout thermo-economic performance by field zoning implementation. American Society of Mechanical Engineers Digital Collection.

[18] Xu C, Wang Z, Li X, Sun F. Energy and exergy analysis of solar power tower plants. Applied Thermal Engineering. 2011;31(17-18):3904-13.

[19] Turchi CS, Ma Z, Neises TW, Wagner MJ. Thermodynamic study of advanced supercritical carbon dioxide power cycles for concentrating solar power systems. Journal of Solar Energy Engineering. 2013;135(4).

[20] Gallardo F, Pratticò L, Toro C. A thermo-economic assessment of CSP+ TES in the north of Chile for current and future grid scenarios. Conference A thermo-economic assessment of CSP+ TES in the north of Chile for current and future grid scenarios, vol. 2126. AIP Publishing LLC, p. 030023.

[21] Hosseini SE, Butler B. Design and analysis of a hybrid concentrated photovoltaic thermal system integrated with an organic Rankine cycle for hydrogen production. J Therm Anal Calorim. 2020;20.

[22] Mehos M, Turchi C, Vidal J, Wagner M, Ma Z, Ho C, et al. Concentrating solar power Gen3 demonstration roadmap. National Renewable Energy Lab.(NREL), Golden, CO (United States); 2017.

565 [23] Nithyanandam K, Pitchumani R. Cost and performance analysis of concentrating solar power
566 systems with integrated latent thermal energy storage. Energy. 2014;64:793-810.

567 [24] Kuravi S, Goswami Y, Stefanakos EK, Ram M, Jotshi C, Pendyala S, et al. Thermal energy
568 storage for concentrating solar power plants. Technology & Innovation. 2012;14(2):81-91.

569 [25] Sukhatme K, Sukhatme S. Solar energy: principles of thermal collection and storage. 1996.
570 Tata McGraw-Hill Education.

571 [26] Collado FJ, Guallar J. Campo: Generation of regular heliostat fields. Renewable energy.
572 2012;46:49-59.

573 [27] Xie Q, Guo Z, Liu D, Chen Z, Shen Z, Wang X. Optimization of heliostat field distribution
574 based on improved Gray Wolf optimization algorithm. Renewable Energy. 2021;176:447-58.

575 [28] Collado FJ, Guallar J. Quick design of regular heliostat fields for commercial solar tower
576 power plants. Energy. 2019;178:115-25.

577 [29] Atif M, Al‐Sulaiman FA. Development of a mathematical model for optimizing a heliostat
578 field layout using differential evolution method. International Journal of Energy Research.
579 2015;39(9):1241-55.

580 [30] Spelling J. Hybrid solar gas-turbine power plants: a thermoeconomic analysis: KTH Royal
581 Institute of Technology, 2013.

582 [31] Bellos E, Pavlovic S, Stefanovic V, Tzivanidis C, Nakomcic‐Smaradgakis BB. Parametric
583 analysis and yearly performance of a trigeneration system driven by solar‐dish collectors.
584 International Journal of Energy Research. 2019;43(4):1534-46.

585 [32] Jadhav S, Venkatraj V. Thermal losses in central receiver solar thermal power plant.
586 Conference Thermal losses in central receiver solar thermal power plant, vol. 377. IOP Publishing,
587 p. 012008.

588 [33] Bejan A. Advanced engineering thermodynamics. Hoboken, New Jersey: John Wiley & Sons,
589 2016.

590 [34] Shaygan M, Ehyaei MA, Ahmadi A, Assad MEH, Silveira JL. Energy, exergy, advanced
591 exergy and economic analyses of hybrid polymer electrolyte membrane (PEM) fuel cell and
592 photovoltaic cells to produce hydrogen and electricity. Journal of Cleaner Production.
593 2019;234:1082-93.

594 [35] Yazdi MRM, Aliehyaei M, Rosen MA. Exergy, economic and environmental analyses of gas
595 turbine inlet air cooling with a heat pump using a novel system configuration. Sustainability.
596 2015;7(10):14259-86.

597 [36] Schwarzbözl P, Buck R, Sugarmen C, Ring A, Crespo MJM, Altwegg P, et al. Solar gas
598 turbine systems: design, cost and perspectives. Solar energy. 2006;80(10):1231-40.

[37] Kolb GJ, Ho CK, Mancini TR, Gary JA. Power tower technology roadmap and cost reduction plan. SAND2011-2419, Sandia National Laboratories, Albuquerque, NM. 2011;7.

[38] Kistler BL. A user's manual for DELSOL3: a computer code for calculating the optical performance and optimal system design for solar thermal central receiver plants. Sandia National Labs., Livermore, CA (USA); 1986.

[39] Saghafifar M. Thermo-economic optimization of hybrid combined power cycles using heliostat solar field. Masters Degree Thesis Submitted at College of Engineering American University of Sharjah. 2016.

[40] Stine WB, Geyer M. Power from the Sun: Power from the sun. net, 2001.

[41] Sandoz R. Thermoeconomic analysis and optimisation of air-based bottoming cycles for water-free hybrid solar gas-turbine power plants. 2012.

[42] Sandoz R, Spelling J, Laumert B, Fransson T. Air-based bottoming-cycles for water-free hybrid solar gas-turbine power plants. Journal of engineering for gas turbines and power. 2013;135(10).

[43] Peters MS, Timmerhaus KD, West RE, Timmerhaus K, West R. Plant design and economics for chemical engineers: McGraw-Hill New York, 1968.

[44] Pitz-Paal R, Dersch J, Milow B. European concentrated solar thermal road-mapping (ECOSTAR). Coordinated action sustainable energy systems SES6-CT-2003-502578 Cologne. 2005.

[45] IEA N. Projected costs of generating electricity. International Energy Agency. 2010;10(02).

[46] Tzivanidis C, Bellos E, Antonopoulos KA. Energetic and financial investigation of a stand-alone solar-thermal Organic Rankine Cycle power plant. Energy conversion and management. 2016;126:421-33.

[47] Shafer T. Calculating inflation factors for cost estimates. City of Lincoln Transportation and Utilities Project Delivery.

[48] Statista. Global inflation rate compared to previous year.

[49] Alvarez-Benitez JE, Everson RM, Fieldsend JE. A MOPSO algorithm based exclusively on pareto dominance concepts. Conference A MOPSO algorithm based exclusively on pareto dominance concepts. Springer, p. 459-73.

[50] Coello CC, Lechuga MS. MOPSO: A proposal for multiple objective particle swarm optimization. Conference MOPSO: A proposal for multiple objective particle swarm optimization, vol. 2. IEEE, p. 1051-6.

[51] Raquel CR, Naval Jr PC. An effective use of crowding distance in multiobjective particle swarm optimization. Conference An effective use of crowding distance in multiobjective particle swarm optimization. p. 257-64.

[52] Collado FJ, Guallar J. A review of optimized design layouts for solar power tower plants with campo code. Renewable and Sustainable Energy Reviews. 2013;20:142-54.

[53] Collado FJ. Preliminary design of surrounding heliostat fields. Renewable energy. 2009;34(5):1359-63.

[54] Sassi G. Some notes on shadow and blockage effects. Solar energy. 1983;31(3):331-3.

[55] Shen C, He Y-L, Liu Y-W, Tao W-Q. Modelling and simulation of solar radiation data processing with Simulink. Simulation Modelling Practice and Theory. 2008;16(7):721-35.

[56] Xu C, Wang Z, Li X, Sun F. Energy and exergy analysis of solar power tower plants. Applied Thermal Engineering. 2011;31(17):3904-13.

[57] Ehyaei M, Bahadori M. Internalizing the social cost of noise pollution in the cost analysis of electricity generated by wind turbines. Wind Engineering. 2006;30(6):521-9.

[58] Weather Atlas.

[59] Nimbalkar S. Waste Heat Recovery from Industrial Process Heating Equipment. Oak Ridge National Laboratory. 2015;20.

[60] Li ZX, Ehyaei MA, Kamran Kasmaei H, Ahmadi A, Costa V. Thermodynamic modeling of a novel solar powered quad generation system to meet electrical and thermal loads of residential building and syngas production. Energy Conversion and Management. 2019;199:111982.

[61] Nakomčić-Smaragdakis BB, Dragutinović NG. Hybrid renewable energy system application for electricity and heat supply of a residential building. Thermal Science. 2016;20(2):695-706.

[62] Asgari E, Ehyaei M. Exergy analysis and optimisation of a wind turbine using genetic and searching algorithms. International Journal of Exergy. 2015;16(3):293-314.

[63] Ehyaei MA, Ahmadi A, Rosen MA. Energy, exergy, economic and advanced and extended exergy analyses of a wind turbine. Energy Conversion and Management. 2019;183:369-81.

[64] Duffie JA, Beckman WA. Solar engineering of thermal processes John Wiley & Sons. Inc New York. 1991.

[65] Ehyaei MA, Ahmadi A, El Haj Assad M, Salameh T. Optimization of parabolic through collector (PTC) with multi objective swarm optimization (MOPSO) and energy, exergy and economic analyses. Journal of Cleaner Production. 2019;234:285-96.

662 [66] Ehyaei MA, Ahmadi A, Assad MEH, Hachicha AA, Said Z. Energy, exergy and economic
663 analyses for the selection of working fluid and metal oxide nanofluids in a parabolic trough
664 collector. Solar Energy. 2019;187:175-84.

665 [67] Jazayeri K, Uysal S, Jazayeri M. MATLAB/simulink based simulation of solar incidence
666 angle and the sun's position in the sky with respect to observation points on the Earth. Conference
667 MATLAB/simulink based simulation of solar incidence angle and the sun's position in the sky
668 with respect to observation points on the Earth. IEEE, p. 173-7.

669 [68] Yao Y, Hu Y, Gao S. Heliostat field layout methodology in central receiver systems based on
670 efficiency-related distribution. Solar energy. 2015;117:114-24.

671